Published in final edited form as:
Comput Biol Med. 2011 October ; 41(10): 936–945. doi:10.1016/j.compbiomed.2011.08.004.

SIMULATING VENTILATION DISTRIBUTION IN HETEROGENOUS LUNG INJURY USING A BINARY TREE DATA STRUCTURE

Ashley A. Colletti[1], **Reza Amini**[1,2], and **David W. Kaczka**[1,2]

[1]Department of Anesthesia, Critical Care, and Pain Medicine, Beth Israel Deaconess Medical Center, Boston, Massachusetts

[2]Harvard Medical School, Boston, Massachusetts

Abstract

To determine the impact of mechanical heterogeneity on the distribution of regional flows and pressures in the injured lung, we developed an anatomic model of the canine lung comprised of an asymmetric branching airway network which can be stored as binary tree data structure. The entire tree can be traversed using a recursive flow divider algorithm, allowing for efficient computation of acinar flow and pressure distributions in a mechanically heterogeneous lung. These distributions were found to be highly dependent on ventilation frequency and the heterogeneity of tissue elastances, reflecting the preferential distribution of ventilation to areas of lower regional impedance.

Keywords

Models; Computational; Models; Biological; Data Structures; Binary Tree; Mechanical Ventilation; Ventilation Distribution; Disease Models; Animal; Elasticity; Lung/pathology/physiopathology; Lung Diseases/pathology/physiopathology; Respiratory Mechanics

INTRODUCTION

Acute Lung Injury (ALI) is a syndrome characterized by the rapid onset of hypoxia and respiratory failure associated with noncardiogenic pulmonary edema, heterogeneous alterations in intrinsic tissue elastance, and atelectasis [1]. Histopathological findings reveal a very heterogeneous inflammatory disruption of alveolar epithelium and transudation of fluid into the air spaces [1]. While endotracheal intubation and mechanical ventilation is the current mainstay of treatment, the heterogeneous mechanical alterations associated with ALI result in a maldistribution of ventilation. In the injured lung, more compliant regions become overventilated and subjected to overdistention [2], while more stiff and flooded regions become underventilated and are at risk for derecruitment [3]. This maldistribution of ventilation results in further inflammation and edema which can worsen the existing injury, especially if high tidal volumes and low end expiratory pressures are used [4]. Protective ventilation strategies relying on low tidal volumes and appropriate positive end-expiratory pressures (PEEPs) can improve mortality in patients with ALI, presumably by recruiting collapsed alveoli, minimizing parenchymal overdistension, and optimizing ventilation distribution [5].

Address correspondence to: David W. Kaczka, M.D., Ph.D. Department of Anesthesia, Critical Care, and Pain Medicine, Beth Israel Deaconess Medical Center, 330 Brookline Avenue, Dana 717A, Boston, MA 02215, Voice: 617 667-0142, Fax: 617 667-1500, dkaczka@bidmc.harvard.edu.

While it has been assumed that the heterogeneous nature of ALI results in maldistribution of ventilation [6], there is little quantitative information as to how flow or pressure may be distributed in this syndrome [7]. The geometry of the airway tree, along with the physical dimensions and properties of its numerous component airway segments and acini, govern how flow is distributed throughout the lung. Given the tremendous structural complexity of this organ, any accurate simulation of ventilation distribution poses a unique and challenging computational problem. For example, many models of the mammalian lung consist of airway segments numbering in the hundreds of thousands [8–11]. Therefore, the goal of this study was to develop a computational data structure to allow for the optimal storage and easy manipulation of the many physical properties associated with individual airway segments in a complex branching network, as well as the efficient determination of pulmonary ventilation distribution using a novel recursive flow-divider algorithm. By further refining the model to account for variable mechanical properties associated with heterogeneous lung injury [12], the model may provide a platform for understanding and optimization of mechanical ventilation protocols in individual patients.

METHODS

Model Overview

The structure of the model was based on the 47-order, asymmetric binary tree cast of the canine lung described by Horsfield et al. [8]. It consists of 300,153 cylindrical airway segments, including 150,077 terminal bronchioles with subtending acini. Each airway segment is assigned a specific order m, denoting its unique cylindrical length and diameter. By the nomenclature of Horsfield et al., the sequential ordering starts at the very terminal bronchioles with $m = 2$, and converges to the highest order at the trachea with $m = 47$. The acini are assigned order $m = 1$. Each airway order is assigned a unique cylindrical length l_m and radius r_m, as well as a recursion index Δ_m to account for branching asymmetry. This Δ_m is defined as the difference between the orders of its two subtending daughter branches [8].

In our model, each airway segment of order m is also characterized by a complex oscillatory longitudinal impedance $Z_{seg,m}$, which incorporates pressure drops associated with viscous flow losses and frequency-dependent velocity profile distortion based on the analysis of Thurston [13]:

$$Z_{seg,m}(\omega)=\left(\frac{j\omega\rho_{air}l_m}{\pi {r_m}^2}\right)\left[1-\frac{2J_1(\alpha_m\sqrt{-j})}{\alpha_m\sqrt{-j}J_0(\alpha_m\sqrt{-j})}\right]^{-1} \quad (1)$$

Here j is the unit imaginary number, ω is the angular frequency, ρ_{air} is air density (1.41×10^{-4} cm H_2O s^2 dm^{-2}), J_0 and J_1 are complex Bessel functions of orders 0 and 1, respectively, and α_m is the so-called Womersley parameter [14], defined as:

$$\alpha_m=r_m\sqrt{\frac{\omega\rho_{air}}{\mu_{air}}} \quad (2)$$

with μ_{air} being the viscosity of air (1.863×10^{-7} cm H_2O s).

To account for flow losses within each airway segment due to viscoelastic wall distention and gas compression, each $Z_{seg,m}$ is partitioned into two equal halves (Figure 1) by a parallel shunt impedance $Z_{shu,m}$:

$$Z_{shu,m}(\omega)=\left[\frac{1-F_{c,m}}{R_{s,m}+j\omega I_{s,m}+\frac{1}{j\omega C_{s,m}}}+\frac{F_{c,m}}{R_{c,m}+j\omega I_{c,m}+\frac{1}{j\omega C_{c,m}}}+j\omega C_{g,m}\right]^{-1} \quad (3)$$

where $F_{c,m}$ is the fractional cartilage content in the wall of an airway segment of order m [15]. The wall resistance (R), inertance (I), and compliance (C) parameters are denoted by subscripts to indicate soft tissue (s) and cartilaginous (c) components, respectively [12]. The $C_{g,m}$ parameter represents the compliance due to the isothermal compression of the gas volume contained within each cylindrical airway segment:

$$C_{g,m}=\frac{\pi r_m^2 l_m}{P_{atm}} \quad (4)$$

with P_{atm} being the ambient pressure at sea level (1033 cm H_2O).

Each of the 150,077 terminal bronchioles is subtended by a unique acinar unit, the fundamental gas exchanging structure of the lung. Each discrete acinus, indexed by n, consists of a viscoelastic tissue element in parallel with a gas compression compliance, the mechanical impedance of which is given by:

$$Z_{acn,n}(\omega)=\left[j\omega C_{g,n}+\frac{\omega^{\alpha}}{(\eta-j)H_n}\right]^{-1} \quad (5)$$

where H_n is tissue elastance, η is tissue hysteresivity [16, 17], $\alpha=(2/\pi)\tan^{-1}(1/\eta)$, and $C_{g,n}$ is the gas compression compliance given by:

$$C_{g,n}=\frac{V_{FRC}}{NP_{atm}} \quad (6)$$

The V_{FRC} is the total lung volume at functional residual capacity, and N is the total number of acini in the model.

Given Horsfield's model structure, the total flow impedance looking into an arbitrary airway segment of order m ($Z_{tot,m}$) can be computed by appropriate serial and parallel additions of its associated longitudinal and shunt impedances (Figure 1) according to the formula:

$$Z_{tot,m}(\omega)=\frac{Z_{seg,m}(\omega)}{2}+\left[\frac{1}{Z_{shu,m}(\omega)}+\frac{1}{\frac{Z_{seg,m}(\omega)}{2}\left[\frac{1}{Z_{tot,m-1}(\omega)}+\frac{1}{Z_{tot,m-1-\Delta_m}(\omega)}\right]^{-1}}\right]^{-1} \quad (7)$$

As a recursive relationship, Equation 7 can be invoked continuously until a terminal bronchiole is reached, at which point the total impedance looking into a terminal airway segment (of order $m = 2$) is given by:

$$Z_{tot,2}(\omega)=\frac{Z_{seg,2}(\omega)}{2}+\left[\frac{1}{Z_{shu,2}(\omega)}+\frac{1}{\frac{Z_{seg,2}(\omega)}{2}+Z_{acn,n}(\omega)}\right]^{-1}. \quad (8)$$

Computing Ventilation Distribution

As the volume of inspired air descends from the trachea to the level of the terminal acini, it divides at each bifurcation in the airway tree. According to Figure 1-A, a portion of the flow entering any airway segment will be lost due to gas compression and airway wall distention [10]. This shunt flow loss, $\dot{V}_{shu,m}$, will depend on the longitudinal airway segment impedance $Z_{seg,m}$, the segment shunt impedance $Z_{shu,m}$, and the total downstream impedances looking into each of the two daughter branches, $Z_{tot,m-1}$ and $Z_{tot,m-1-\Delta m}$:

$$\dot{V}_{shu,m}(\omega)=\left(\frac{\frac{Z_{seg,m}(\omega)}{2}+\left[\frac{1}{Z_{tot,m-1}(\omega)}+\frac{1}{Z_{tot,m-1-\Delta_m}(\omega)}\right]^{-1}}{Z_{shu,m}(\omega)+\frac{Z_{seg,m}(\omega)}{2}+\left[\frac{1}{Z_{tot,m-1}(\omega)}+\frac{1}{Z_{tot,m-1-\Delta_m}(\omega)}\right]^{-1}}\right)\dot{V}_{in,m}(\omega) \tag{9}$$

where $\dot{V}_{in,m}$ denotes the flow entering the segment of order m. The $\dot{V}_{shu,m}$ can further be partitioned into components corresponding to airway wall distention ($\dot{V}_{w,m}$), as well as the compression of gas contained within the airway segment ($\dot{V}_{Cg,m}$):

$$\dot{V}_{w,m}(\omega)=\left[\frac{1}{j\omega C_{g,n}Z_{shu,m}(\omega)}\right]\dot{V}_{shu,m}(\omega) \tag{10}$$

$$\dot{V}_{Cg,m}(\omega)=\dot{V}_{shu,m}(\omega)-\dot{V}_{w,m}(\omega) \tag{11}$$

Thus, the flow leaving the airway segment, $\dot{V}_{out,m}$, will be given by:

$$\dot{V}_{out,m}(\omega)=\dot{V}_{in,m}(\omega)-\dot{V}_{shu,m}(\omega) \tag{12}$$

At any bifurcation in the airway tree, the subtending daughter impedances $Z_{tot,m-1}$ and $Z_{tot,m-1-\Delta m}$ will determine flow partitioning:

$$\dot{V}_{in,m-1}(\omega)=\left[\frac{Z_{tot,m-1-\Delta_m}(\omega)}{Z_{tot,m-1}(\omega)+Z_{tot,m-1-\Delta_m}(\omega)}\right]\dot{V}_{out,m}(\omega) \tag{13}$$

$$\dot{V}_{in,m-1-\Delta_m}(\omega)=\left[\frac{Z_{tot,m-1}(\omega)}{Z_{tot,m-1}(\omega)+Z_{tot,m-1-\Delta_m}(\omega)}\right]\dot{V}_{out,m}(\omega) \tag{14}$$

where $\dot{V}_{in,m-1}$ and $\dot{V}_{in,m-1-\Delta_m}$ are the flows entering the daughter branches of orders $m-1$ and $m-1-\Delta_m$, respectively.

At the level of the terminal bronchioles (Figure 1-B), the flow lost to gas compression and wall distention within any order 2 airway segment is given by:

$$\dot{V}_{shu,2}(\omega)=\left(\frac{Z_{seg,2}(\omega)+2Z_{acn,n}(\omega)}{2Z_{shu,2}(\omega)+Z_{seg,2}(\omega)+2Z_{acn,n}(\omega)}\right)\dot{V}_{in,2}(\omega) \tag{15}$$

Thus the flow leaving an order 2 segment and entering an acinus is given by:

$$\dot{V}_{out,2}(\omega)=\dot{V}_{in,2}(\omega)-\dot{V}_{shu,2}(\omega) \tag{16}$$

which will be partitioned between parenchymal tissue distension ($\dot{V}_{ti,n}$) and acinar gas compression($\dot{V}_{Cg,n}$):

$$\dot{V}_{ti,n}(\omega)=\left[\frac{1}{1+j\omega^{1-\alpha}C_{g,n}(\eta-j)H_n}\right]\dot{V}_{out,2}(\omega) \tag{17}$$

$$\dot{V}_{Cg,n}(\omega)=\dot{V}_{out,2}(\omega)-\dot{V}_{ti,n}(\omega) \tag{18}$$

Finally, the distending pressure at any acinus can be obtained as:

$$P_{acn,n}(\omega)=Z_{acn,n}(\omega)\ \dot{V}_{out,2}(\omega) \tag{19}$$

Data Structure

For the purposes of computing the global mechanics of a heterogeneous lung model, the total impedance looking into the tracheal opening (Z_L) can be obtained using simple recursive function calls according to Equations 7 and 8, and thus does not require any additional data storage in memory beyond the lengths, radii, and recursion indices associated with a particular airway segment order [12]. All airway segment impedances can be computed as needed according to Equations 1 and 3, and acinar impedances with stochastically variable elastances can be determined with simple random number draws. However the subsequent computation of flow and pressure distributions throughout such an asymmetric branching network, with heterogeneously distributed airway or tissue impedances, requires that the exact model structure be explicitly defined and stored in computer random access memory, such that flow partitioning can be performed according to Equations 9 – 18. For this, we developed a binary tree data structure consisting of multiple nodes representing specific airway segments. Each node in the tree consists of a data record to store the order of its corresponding airway segment, the value of the total impedance looking into this segment, as well as two pointers linking itself to two daughter nodes (Figure 2). Any node corresponding to a terminal bronchiole (i.e., $m = 2$) points only to its unique acinar structure [8].

Each of the 300,153 nodes in our tree is assigned using a unique key identifier, the value of which is determined according to a recursive algorithm. Assuming an arbitrary airway segment of order m is assigned a key value k_m, the keys corresponding to its $m-1$ and $m-1-\Delta_m$ daughter nodes are computed as:

$$k_{m-1}=k_m-2^{m-1} \tag{20}$$

$$k_{m-1-\Delta_m}=k_m+2^{m-1-\Delta_m} \tag{21}$$

Figure 3 shows the assigned key values for a portion of an example $M = 8$ generation tree, assuming $\Delta_m = 1$ for all orders. To start the algorithm, the root node in this case is assigned

key value $2^7 = 128$, while its left and right daughter branches are assigned key values $128-2^{7-1}=64$ and $128+2^{7-1-1}=160$, respectively, according to Equations 20 and 21.

Simulations

All simulations were performed assuming a 25 kg dog with V_{FRC} = 40 ml kg^{-1}. The airway segment lengths, diameters, recursion indices, and wall properties (with appropriate cartilaginous and soft tissue distributions) for each order were assigned as previously described [8, 12, 15, 18]. To mimic the diffuse mechanical heterogeneity of the acutely injured lung [7], we allowed the value of each acinar tissue elastance H_n to vary stochastically according to a uniform probability distribution function, with H_{min} and H_{max} denoting its upper and lower bounds, respectively [12]. Four different physiologic/pathologic conditions were simulated by appropriate selections of H_{min} and H_{max}. All conditions assumed a fixed value of $H_{min} = 20N$ cm H_2O L^{-1}, but the value of H_{max} was varied to correspond to a completely healthy canine lung with homogeneous tissues, a canine lung with mild tissue heterogeneity, as well as moderate and severe lung injury (Table 1). The hysteresivity parameter η for each acinus (Equation 5) was assumed to have a constant value of 0.2 independent of H_n, in accordance with the structural damping hypothesis [16]. Input impedance at the trachea, as well as acinar flow and pressure distributions, were computed for discrete, sinusoidal flow forcings at frequencies of 0.01, 0.10, 0.33, 1.0, 3.0, 10, 20, 33, 50, and 100 Hz. This frequency range, which is inclusive of rates corresponding to conventional ventilation [19] as well as high frequency oscillation [20], was chosen for its sensitivity to the effects of heterogeneous airway and tissue properties [7, 10, 12, 21]. For each condition, we also computed the flow and pressure distributions at the lung resonant frequencies (f_r) as determined from the zero crossings in the reactive component of Z_L [12].

Recursive computational algorithms for generating the airway tree, computing and storing input impedances, and determining flow divisions were performed using a standard preorder traversal sequence [22]. The algorithms were written and executed using MATLAB v7.0 (The Mathworks, Natick, MA) and the *Data Structures and Algorithms Toolbox* (available online at http://code.google.com/p/pointer/). Flow division was determined at every node in the tree according to Equations 9, 12, 13, and 14. Total computation time for each simulation was approximately one hour on a Dell desktop computer with an Intel Pentium® 4 processor operating at 2.80 GHz with 2.99 GB RAM. As all impedances within the tree were complex values with both real and imaginary components, all flows and pressures were also complex quantities. However, we expressed these in polar coordinates (i.e., amplitudes and phases) for the purposes of our analyses.

To quantify the total flow lost to gas compression and airway wall distention as functions of frequency and disease condition, the shunt flows at each node were partitioned according to Equations 10, 11, and 18. At the very terminal nodes, we determined the portion of flow available for useful acinar ventilation according to Equation 17. The complex components of these flows were then summed and normalized by the corresponding input tracheal flow to yield the net acinar flow, net gas compression flow, and net airway wall distention flow.

To further quantify the heterogeneity of ventilation distribution, we examined the amplitude and phase histograms of acinar flows and pressures for each disease condition. Acinar flow amplitudes were normalized relative to what those values would be for a perfectly symmetric, homogeneous lung with rigid airway walls and no gas compression [10], while the pressure amplitudes were normalized relative to tracheal pressure. The phases for both acinar flows and pressures were normalized relative to the corresponding tracheal phase, constrained to be within ±180°. Bin sizes for the normalized flow and pressure amplitudes were 0.025 and 0.005, respectively, and 1 degree for the phases.

RESULTS

Figure 4 shows the mechanical impedance spectra as observed from the trachea (i.e., whole lung impedance, Z_L) for the four different pathologic conditions of Table 1. This Z_L is expressed as lung resistance (R_L), reactance (X_L), and elastance ($E_L = -2\pi f X_L$). Since the inertia of gas in the central airways begins to influence X_L for frequencies above 1 Hz, E_L is plotted only for frequencies between 0.01 and 1.0 Hz. Regardless of disease condition R_L decreased with increasing frequency from 0.01 to 10 Hz, but increased as frequency increased above 10 Hz. The E_L exhibited a positive dependence on frequency over the observed range of 0.01 to 1.0 Hz. Consistent with experimental studies of canine lung injury [7], we also observed that both R_L and E_L increased at each frequency with increasing acinar heterogeneity (i.e., disease severity). The corresponding resonant frequencies, as determined from the zero crossings of X_L, increased with disease severity (Table 2).

Figure 5 shows the effect of frequency on the relative magnitudes and phases of the net acinar tissue flow (Equation 17), net gas compression flow (Equations 11 and 18), and net airway wall distension flow (Equation 10) for the four different pathologic conditions. Regardless of frequency, increasing lung tissue heterogeneity corresponded to decreases in the magnitude of net acinar tissue flow, but increases in gas compression and airway wall distention flows. Moreover, these net flows became increasingly out of phase with the tracheal flow as frequency increased above 10 Hz.

Figure 6 shows the distribution of normalized acinar flow amplitudes and phases for each of the four simulated pathologic conditions. For clarity, histograms are shown only for frequencies of 1.0, 10, 20, 50, and 100 Hz, as we observed minimal differences in the shapes of the distributions between 0.01 to 1.0 Hz. Moreover, the flow distributions at the resonant frequencies for each condition were indistinguishable from those at 10 Hz. The distribution of acinar flow magnitudes widened as ventilation frequency increased. The shape of these acinar flow distributions tended to become more hyperbolic as the severity of the simulated injury increased. In general, the widening of these flow distributions indicated considerably more regions of under- and over-ventilation with increasing tissue heterogeneity and disease severity, as determined from the number of acini receiving normalized flows below or above 1, respectively. Similarly for each condition, the distribution of phases also widened with increasing frequency, with the most acini demonstrating tremendous ventilation asynchrony at 20 Hz. However, the spread of the phases at a given frequency generally decreased with increasing tissue heterogeneity.

Figure 7 shows the distribution of acinar pressures for the four conditions at the same five frequencies from Figure 6, as well as the resonant frequency (Table 2). At frequencies of 1 Hz or lower, acinar pressures demonstrated minimal differences in amplitudes and phases compared to tracheal pressure, regardless of disease condition. However at the resonant frequency, the distribution widths increased for both pressure amplitudes and phases. The acinar pressures also exhibited amplification relative to tracheal pressure at the resonant frequency, and the corresponding phase distributions were centered around −90°. Moreover, the degree of amplification increased with increasing disease severity. At 10 Hz, the distribution of acinar pressure amplitudes were lower compared to tracheal pressure for the two healthy conditions, but were amplified for severe injury. At 20 Hz and above, the acinar pressure amplitudes became progressively more attenuated, and the corresponding phase distributions ranged mostly from 0° to 180°.

DISCUSSION

In this study, we present the use of a data structure for the efficient computer memory storage of a complex biological tree, as well as the computation of oscillatory flows and pressures throughout a heterogeneous mammalian lung. In our model structure, we adopted the asymmetric canine airway network of Horsfield et al. [8], which orders the bronchial tree starting from the terminal tissue elements (order 1) up to the trachea (order 47). In this model, any two subtending daughter branches sharing the parent branch may be of different orders, as defined by the recursion index Δ_m. Horsfield et al. originally assigned specific diameters, lengths, and recursion indices to each order [8], assuming that airway segment dimensions for any given order were identical (i.e., self-consistent). Such an arrangement allows for efficient calculations of impedance and ventilation distribution along just one pathway, connecting a single acinus to the trachea, since the mechanical properties of the subtree looking into any specified node will be identical to that of all other nodes with the same order. Thus this model has seen much use for the calculation of physiologic variables such as input impedance [15], acoustic transmission [9], as well as flow and pressure distributions [23, 24].

However when structural or functional heterogeneities are imposed on the model, such as variable alterations in airway dimensions [18] or parenchymal elastances [12], the computational efficiency arising from the self-similarity of the airway tree is lost. Thus any forward model simulation of ventilation distribution in a mechanically heterogeneous lung requires that the tree by explicitly defined and stored in computer memory [25]. Our approach was to develop a data structure based on a binary tree that would allow for easy access to the local mechanical properties and efficient flow partitioning at every node in a heterogeneous tree using a recursive preorder tree traversal sequence [22]. This has particular relevance to simulating ventilation distribution in the acutely injured lung, which often exhibits heterogeneous mechanical properties [7, 26] and is predisposed to ventilator-associated lung injury due to parenchymal overdistention and atelectrauma [27, 28]. While this approach differs from other computational modeling techniques based on imaging data [11, 29, 30], we believe a binary tree is an ideal data structure for the recursive, complex arithmetic operations associated with oscillatory flow and pressure divisions in such a hierarchical network.

Similar to a previous modeling study from our group [12], we constructed an injured canine lung by allowing for stochastic variations acinar tissue elastances that could mimic the alterations observed in whole-lung mechanical impedance measurements [7]. However for simplicity, we assumed that the values of these acinar elastances were uniformly distributed over ranges bounded by $H_{\min}$ and $H_{\max}$. Our model reproduces typical impedance spectra observed experimentally in both healthy and injured canine lungs (Figure 4), including the enhanced negative frequency dependence in R_L for frequencies below 10 Hz due to the combined effects of viscoelasticity and parallel time constant heterogeneity [31]. Our simulations also reproduce the positive frequency dependence of R_L between 10 to 100 Hz, which in canine lungs may arise from the known antiresonance between tissue inertia (Equation 3) and gas compression compliance (Equations 4 and 6) [32]. As expected, total lung elastance E_L demonstrated a positive dependence on frequency due to viscoelasticity [33]. However the values of E_L at each frequency increased with disease severity, since the effective (or average) lung tissue elastance increased with the value $H_{\max}$ [12]. Such increases in E_L also contribute to increased resonant frequency f_r with disease severity, since $f_r = \left(\sqrt{E_L/I_L}\right)/2\pi$, with I_L being the effective lung inertance [34].

As expected, our data demonstrate that the net flow lost to gas compression and airway wall distention increases with: 1) disease severity, as parenchymal stiffness increases; and 2)

ventilator frequency, as the shunt impedances offered by the airway walls and gas contained within the lung decrease. This results in net decreases in the flow delivered to the acini. Indeed for our severe lung injury condition, only 60–80% of the flow at the airway opening may be available for useful gas exchange, depending on frequency (Figure 5). More importantly, our simulations highlight the important relationships between ventilation frequency and the heterogeneity of parenchymal stiffness on the distribution and synchrony of acinar ventilation. These relationships indicate that for a specified level of parenchymal heterogeneity, the distribution of acinar flow becomes more heterogeneous and asynchronous as ventilation frequency increases, especially over ranges typically used in high frequency oscillation (Figure 6). Increases in the width of the flow amplitude distribution implies that more regions of the lung are subjected to under-ventilation and poor gas exchange, as well as over-ventilation with potential for volutrauma [10]. This is consistent with the notion that ventilation will be partitioned preferentially to areas of the lung with lower regional impedances, while being decreased to areas of higher impedance.

However, increases in the width of the acinar phase distribution implies enhanced pendelluft and interregional gas mixing [35], which may be an important mechanism for gas exchange during high frequency, low amplitude ventilation [36]. Indeed, our simulations are both qualitatively and quantitatively similar to the results reported by Lehr et al. using stroboscopic photography of pleural surface motion in excised dog lungs during flow oscillations from 1 to 30 Hz [35]. While they speculated that such asynchronous flows can arise from parenchymal wave phenomena [37], our model does not incorporate any mechanisms for wave transmission through a viscoelastic solid. Thus any heterogeneity in the distribution of flow amplitudes and phases we observed must be attributed to variations in regional time constants. Certainly for our healthy, homogeneous condition, such time constant variations arise from the distribution of pathlengths from trachea to acini [9]. In the heterogeneously injured lung, we observed increases in the widths of the flow amplitude distributions for any given frequency with increasing parenchymal tissue heterogeneity. However the observed phase distributions at a given frequency tended to become more narrow as the level of simulated injury increased. This may seem counterintuitive, but we point out that for our simulations, increasing disease severity also corresponded to an increase in average acinar elastance (i.e., $(H_{min}+H_{max})/2$ in our model). Such an increase in effective tissue stiffness can make ventilation distribution more synchronous, as has been demonstrated experimentally by other investigators using alveolar capsules in different species [38–40].

Our analysis follows a previous modeling study by Gillis and Lutchen [10], who predicted ventilation distribution from 0.1 to 5 Hz during heterogeneous bronchoconstriction in an asymmetrically branching model of the human lung [24]. Similar to our present study, they determined that flow distribution may become uneven in obstructive lung diseases such as asthma, with implication for parenchymal damage at during ventilation at physiologic breathing rates. Nonetheless, this study did not address how flow and pressure may be distributed in an injured lung with pathologic variations in tissue elastance, or over frequency ranges typically used for high frequency oscillation.

Also consistent with previously published alveolar capsule studies [38–42], our model predicts that the amplitudes of acinar pressure swings will be nearly uniform and identical to tracheal pressure for frequencies below resonance, but will become more heterogeneous and amplified compared to the airway opening as the resonant frequency is approached (Figure 7). Our model predicts that such amplification will become enhanced as the severity of lung injury increases, again most likely due to the increases in average acinar elastance [38, 39]. However above resonance, alveolar pressure becomes rapidly attenuated relative to the airway opening, as most of the pressure drop across the lungs at these higher frequencies is

due to the resistance and inertia of gas in the central airways [40]. Indeed our simulations demonstrate that at 50 and 100 Hz, the amplitude of acinar pressures swings are negligible. Allen and coworkers quantified the heterogeneity of mean alveolar pressure during high frequency oscillation in dogs and rabbits [38, 39], and also observed increasing interregional heterogeneity of alveolar pressures at high frequency. Our results are in agreement with the findings of these studies.

Some important limitations of this modeling approach to predict ventilation distribution should be noted. For the purposes of these simulations, we assumed that the dynamic behavior of the lung is linear and stationary during oscillatory flow excitations. Thus caution should be exercised when extrapolating our results to large variations in tidal volume or airway pressure that may result in intratidal changes in airway segment dimensions, turbulent airflow patterns, parenchymal overdistention, or cyclic recruitment and derecruitment. While our data structure does not preclude the incorporation of such nonlinear or nonstationary phenomena into a model of the injured lung, it would require considerably more computational time. In addition, our model does not include mechanisms for airway-tissue interdependence or collateral ventilation, both of which have the potential to be important determinants of ventilation distribution in some species [43–45]. Finally, while the branching network of Horsfield et al. accurately describes the morphometric and statistical properties of the canine airway tree [8], it is in fact a one-dimensional representation of the dog lung, and thus lacks explicit anatomic detail [11]. Nonetheless, our model could be enhanced such that each airway segment or acinus is assigned a unique location in three-dimensional space [29, 30, 46], allowing for further simulations incorporating pathology in anatomically distinct regions or topographic variation such as lung height or apex-to-base locations.

We chose to perform these simulations using a dog lung model, based on extensive archived information of anatomic and physiologic data in canine lungs [8, 23, 32, 47–50], especially during acute lung injury [7, 26, 51, 52]. Moreover the dog is sufficiently large in size such that its pulmonary mechanics scale appropriately to humans, making these results generalizable to patients with lung injury. These simulations may therefore have clinical relevance for the selection of appropriate frequencies in conventional ventilation or high frequency oscillation based on the degree of lung injury, the relative portions of over- and under-ventilated lung parenchyma, as well as interregional gas mixing.

SUMMARY

We developed a computational model of the canine lung comprised of an asymmetric branching airway network which is stored in a binary tree data structure. The nodes in the tree account for viscous dissipation and convective acceleration of gas flow in cylindrical airway conduits, as well as viscoelastic airway walls and parenchymal tissues. To assess regional ventilation to the individual acini, the entire binary tree can be traversed using a recursive flow divider algorithm, allowing for the computation of acinar flow and pressure distributions. These distributions are highly dependent on regions of maximal tissue stiffness and the heterogeneity of tissue elastances, reflecting preferential distribution of ventilation to areas of lower impedance and decreased flow to areas of higher impedance. Such ventilatory imbalances may be responsible for the organ-level pathophysiology observed during positive pressure ventilation in acute lung injury. Moreover, our model demonstrates that global lung resistance and elastance assessed at the airway opening is highly dependent on parenchymal tissue heterogeneity and ventilation frequency. We conclude that the heterogeneity of regional lung mechanics is an important determinant of ventilation distribution and gas exchange, especially in the acutely injured lung. The results demonstrate that computational modeling of ventilation distribution in the injured lung has

the potential to assist in the development of less injurious conventional and oscillatory ventilation strategies.

Acknowledgments

Supported by NIH Grant HL089227. The authors thank Dr. Brett Simon for his helpful criticisms of the manuscript.

GLOSSARY/NOMENCLATURE

ALI	acute lung injury
$C_{g,m}$	gas compression compliance for airway segment of order *m*
$C_{g,n}$	gas compression compliance of acinus *n*
$C_{s,m}$, $C_{c,m}$	soft tissue and cartilaginous components of airway wall compliance, respectively
E_L	total lung elastance
$F_{c,m}$	fractional cartilage content in wall of airway segment of order *m*
f	oscillation frequency in Hz
h_m	wall thickness for airway segment of order *m*
H_n	tissue elastance of acinus *n*
H_{min}	minimum value of tissue elastance
H_{max}	maximum value of tissue elastance
I_L	effective lung inertance
$I_{s,m}$, $I_{c,m}$	soft tissue and cartilaginous components of airway inertance compliance, respectively
j	unit imaginary number (i.e., $\sqrt{-1}$)
J_x	complex Bessel function of order *x*
k	key identifier for node in binary tree
l_m	airway segment length of order *m*
m	airway segment Horsfield order
n	acinar index
N	total number of acini in the model (150,077)
P_{atm}	ambient pressure (1033 cm H_2O)
$P_{acn,n}$	distending pressure for acinus *n*
PEEP	positive end-expiratory pressure
r_m	airway segment radius of order *m*
R_L	total lung resistance
$R_{s,m}$, $R_{c,m}$	soft tissue and cartilaginous components of airway wall resistance, respectively
V_{FRC}	lung volume at functional residual capacity
$V_{seg,m}$	volume of air contained in airway segment of generation *m*

$\dot{V}_{Cg,n}$	flow lost to compression of gas contained in acinus *n*
$\dot{V}_{in,m}$	flow entering airway segment of order *m*
$\dot{V}_{out,m}$	flow exiting airway segment of order *m*
$\dot{V}_{shu,m}$	flow lost to gas compression and wall distention in airway segment of order *m*
$\dot{V}_{ti,n}$	flow distending parenchymal tissues of acinus *n*
X_L	total lung reactance
Z_L	total lung impedance
$Z_{acn,n}$	impedance of acinus *n*
$Z_{seg,m}$	longitudinal impedance for airway segment of order *m*
$Z_{shu,m}$	parallel shunt impedance for airway segment of order *m*
$Z_{tot,m}$	total impedance looking into airway segment of order *m*
α_m	Womersley parameter for airway segment of order *m*
α	oscillation frequency exponent
Δ_m	recursion index for airway segment of order *m*
η	tissue hysteresivity
μ_{air}	viscosity of air (1.863×10^{-7} cm H_2O s)
ρ_{air}	density of air (1.41×10^{-4} cm H_2O s^2 dm^{-2})
ω	angular oscillation frequency in radians sec^{-1}

References

1. Ware LB, Matthay MA. The Acute Respiratory Distress Syndrome. N Engl J Med. 2000; 342:1334–1349. [PubMed: 10793167]
2. Nucci G, Suki B, Lutchen K. Modeling airflow-related shear stress during heterogeneous constriction and mechanical ventilation. J Appl Physiol. 2003; 95:348–356. [PubMed: 12651864]
3. Karmrodt J, Bletz C, Yuan S, et al. Quantification of atelectatic lung volumes in two different porcine models of ARDS. Br J Anaesth. 2006; 97(6):883–895. [PubMed: 17046849]
4. Amato MB, Barbas CS, Medeiros DM, et al. Beneficial effects of the “open lung approach” with low distending pressures in acute respiratory distress syndrome. A prospective randomized study on mechanical ventilation. Am J Resp Crit Care Med. 1995; 152:1835–1846. [PubMed: 8520744]
5. The ARDS Network. Ventilation with lower tidal volumes as compared with traditional tidal volumes for acute lung injury and the acute respiratory distress syndrome. N Engl J Med. 2000; 342(18):1301–1308. [PubMed: 10793162]
6. Bellardine-Black CL, Hoffman AM, Tsai L, et al. Relationship between dynamic respiratory mechanics and disease heterogeneity in sheep lavage injury. Crit Care Med. 2007; 35(3):870–878. [PubMed: 17255854]
7. Kaczka DW, Hager DN, Hawley ML, et al. Quantifying mechanical heterogeneity in canine acute lung injury: Impact of mean airway pressure. Anesthesiology. 2005; 103:306–317. [PubMed: 16052113]
8. Horsfield K, Kemp W, Phillips S. An asymmetrical model of the airways of the dog lung. J Appl Physiol. 1982; 52(1):21–26. [PubMed: 7061267]
9. Fredberg JJ, Hoenig A. Mechanical response of the lungs at high frequencies. J Biomech Eng. May. 1978 100:57–66.

10. Gillis HL, Lutchen KR. How heterogeneous bronchoconstriction affects ventilation distribution in human lungs: a morphometric model. Ann Biomed Eng. 1999; 27:14–22. [PubMed: 9916756]
11. Tawhai MH, Hunter P, Tschirren J, et al. CT-based geometry analysis and finite element models of the human and ovine bronchial tree. J Appl Physiol. 2004; 97(6):2310–2321. [PubMed: 15322064]
12. Kaczka DW, Massa CB, Simon BA. Reliability of estimating stochastic lung tissue heterogeneity from pulmonary impedance spectra: a forward-inverse modeling study. Ann Biomed Eng. 2007; 35(10):1722–1738. [PubMed: 17558554]
13. Thurston GB. Periodic fluid flow through circular tubes. J Acoust Soc Am. 1952; 24(6):653–656.
14. Womersley JR. Method for the calculation of velocity, rate of flow and viscous drag in arteries when the pressure gradient is known. J Physiol. 1955; 127:553–563. [PubMed: 14368548]
15. Habib RH, Suki B, Bates JHT, et al. Serial distribution of airway mechanical properties in dogs: effects of histamine. J Appl Physiol. 1994; 77(2):554–566. [PubMed: 8002500]
16. Fredberg JJ, Stamenovic D. On the imperfect elasticity of lung tissue. J Appl Physiol. 1989; 67(6): 2048–2419.
17. Hantos Z, Daroczy B, Suki B, et al. Input impedance and peripheral inhomogeneity of dog lungs. J Appl Physiol. 1992; 72(1):168–178. [PubMed: 1537711]
18. Lutchen KR, Gillis H. Relationship between heterogeneous changes in airway morphometry and lung resistance and elastance. J Appl Physiol. 1997; 83(4):1192–1201. [PubMed: 9338428]
19. Kaczka DW, Barnas GM, Suki B, et al. Assessment of time-domain analyses for estimation of low-frequency respiratory mechanical properties and impedance spectra. Ann Biomed Eng. 1995; 23:135–151. [PubMed: 7605051]
20. Kaczka DW, Lutchen KR. Servo-controlled pneumatic pressure oscillator for respiratory impedance measurements and high frequency ventilation. Ann Biomed Eng. 2004; 32(4):596–608. [PubMed: 15117033]
21. Kaczka DW, Lutchen KR, Hantos Z. Emergent behavior of regional heterogeneity in the lung and its effects on respiratory impedance. J Appl Physiol. 2011; 110(5):1473–1481. [PubMed: 21292840]
22. Knuth, D. The Art of Computer Programming. 3. Addison-Wesley; 1997.
23. Jackson AC, Tabrizi M, Kotlikoff MI, et al. Airway pressures in an asymmetrically branched airway model of the dog respiratory system. J Appl Physiol. 1984; 57(4):1223–1230. [PubMed: 6438032]
24. Fredberg JJ, Moore JA. The distributed response of complex branching duct networks. J Acoust Soc Am. 1978; 63(3):954–961. [PubMed: 670560]
25. Thorpe CW, Bates JHT. Effect of stochastic heterogeneity on lung impedance during acute bronchoconstriction: a model analysis. J Appl Physiol. 1997; 82(5):1616–1625. [PubMed: 9134912]
26. Kaczka DW, Cao K, Christensen GE, et al. Analysis of regional mechanics in canine lung injury using forced oscillations and 3D image registration. Ann Biomed Eng. 2011; 39(3):1112–1124. [PubMed: 21132371]
27. Martynowicz MA, Minor TA, Walters BJ, et al. Regional expansion of oleic acid-injured lungs. Am J Resp Crit Care Med. 1999; 160(1):250–258. [PubMed: 10390408]
28. Martynowicz MA, Walters BJ, Hubmayr RD. Mechanisms of recruitment in oleic acid-injured lungs. J Appl Physiol. 2001; 90(5):1744–1753. [PubMed: 11299264]
29. Martonen TB, Isaacs K, Hwang D. Three-dimensional simulations of airways within human lungs. Cell Biochem Biophys. 2005; 42:223–249. [PubMed: 15976457]
30. Martonen TB, Yang Y, Hwang D, et al. Computer simulations of human lung structures for medical applications. Comput Biol Med. 1995; 25(5):431–446. [PubMed: 8575158]
31. Lutchen KR, Hantos Z, Petak F, et al. Airway inhomogeneities contribute to apparent lung tissue mechanics during constriction. J Appl Physiol. 1996; 80(5):1841–1849. [PubMed: 8727575]
32. Jackson AC, Lutchen KR. Physiological basis for resonant frequencies in respiratory system impedance in dogs. J Appl Physiol. 1991; 70(3):1051–1058. [PubMed: 2032970]
33. Suki B, Barabasi AL, Lutchen KR. Lung tissue viscoelasticity: a mathematical framework and its molecular basis. J Appl Physiol. 1994; 76(6):2749–2759. [PubMed: 7928910]

34. Peslin, R.; Fredberg, JJ. Handbook of Physiology. Bethesda: American Physiological Society; 1986. Oscillation mechanics of the respiratory system; p. 145-177.
35. Lehr JL, Butler JP, Westerman PA, et al. Photographic measurement of pleural surface motion during lung oscillation. J Appl Physiol. 1985; 59(2):623–633. [PubMed: 4030616]
36. Chang HK. Mechanisms of gas transport during ventilation by high-frequency oscillation. J Appl Physiol. 1984; 56(3):553–563. [PubMed: 6368498]
37. Butler JP, Lehr JL, Drazen JM. Longitudinal elastic wave propagation in pulmonary parenchyma. J Appl Physiol. 1987; 62(4):1349–1355. [PubMed: 3597210]
38. Allen JL, Fredberg JJ, Keefe DH, et al. Alveolar pressure magnitude and asynchrony during high-frequency oscillations of excised rabbit lungs. Am Rev Respir Dis. 1985; 132(2):343–349. [PubMed: 4026057]
39. Allen JL, Frantz I, Fredberg JJ. Heterogeneity of mean alveolar pressure during high-frequency oscillations. J Appl Physiol. 1987; 62(1):223–228. [PubMed: 3558183]
40. Fredberg JJ, Keefe DH, Glass GM, et al. Alveolar pressure nonhomogeneity during small-amplitude high-frequency oscillation. J Appl Physiol. 1984; 57(3):788–800. [PubMed: 6490465]
41. Fredberg JJ, Allen J, Tsuda A, et al. Mechanics of the respiratory system during high frequency ventilation. Acta Anaesthesiol Scand Suppl. 1989; 90:39–45. [PubMed: 2648738]
42. Warner DO. Alveolar pressure inhomogeneity during low-frequency oscillation of excised canine lobes. J Appl Physiol. 1990; 69(1):155–161. [PubMed: 2394645]
43. Macklem PT. Airway obstruction and collateral ventilation. Physiol Rev. 1971; 51(2):368–436. [PubMed: 4928122]
44. Woolcock AJ, Macklem PT. Mechanical factors influencing collateral ventilation in human, dog, and pig lungs. J Appl Physiol. 1971; 30(1):99–115. [PubMed: 5538799]
45. Anafi RC, Wilson TA. Airway stability and heterogeneity in the constricted lung. J Appl Physiol. 2001; 91:1185–1192. [PubMed: 11509514]
46. Martonen TB, Hwang D, Guan X, et al. Supercomputer description of human lung morphology for imaging analysis. J Nucl Med. 1998; 39(4):745–750. [PubMed: 9544692]
47. Barnas GM, Stamenovic D, Lutchen KR, et al. Lung and chest wall impedances in the dog: effects of frequency and tidal volume. J Appl Physiol. 1992; 72(1):87–93. [PubMed: 1537748]
48. Woldehiwot Z, Horsfield K. Diameter, length and branching angles of the upper airways in the dog lung. Respir Physiol. 1978; 33(2):213–218. [PubMed: 694247]
49. Jackson AC, Lutchen KR, Dorkin HL. Inverse modeling of dog airway and respiratory system impedances. J Appl Physiol. 1987; 62(6):2273–2282. [PubMed: 3610923]
50. Lutchen KR, Jackson AC. Effects of tidal volume and methacholine on low-frequency total respiratory impedance in dogs. J Appl Physiol. 1990; 68(5):2128–2138. [PubMed: 2193908]
51. Barnas GM, Stamenovic D, Lutchen KR. Lung and chest wall impedances in the dog in normal range of breathing: effects of pulmonary edema. J Appl Physiol. 1992; 73(3):1040–1046. [PubMed: 1400015]
52. Barnas GM, Sprung J, Kahn R, et al. Lung tissue and airway impedance during pulmonary edema in the normal range of breathing. J Appl Physiol. 1995; 78(5):1889–1897. [PubMed: 7649927]

Biographies

Ashley A. Colletti received the B.S. degree in biomedical engineering from The Johns Hopkins University in Baltimore, MD in 2009. In 2010, she was employed as a research assistant in the Department of Anesthesia, Critical Care, and Pain Medicine at Beth Israel Deaconess Medical Center in Boston, MA. She is currently a candidate for the M.D. degree at the University of Toledo College Of Medicine, Toledo, OH.

Reza Amini received his Ph.D. in mechanical engineering from Northeastern University in Boston, MA in 2007. He was a postdoctoral research fellow in the Department of Anesthesiology & Critical Care Medicine at The Johns Hopkins University in Baltimore, MD. He is currently a research fellow at Beth Israel Deaconess Medical Center and Harvard

Medical School in Boston, MA. His research interest includes computer modeling of lung mechanics and ventilatory management in acute lung injury.

David W. Kaczka is an Assistant Professor of Anasthesia at Harvard Medical School and a staff anesthesiologist at Beth Israel Deaconess Medical Center in Boston, MA. He received the B.S. (*summa cum laude*), M.S., and Ph.D. degrees in biomedical engineering from Boston University College of Engineering in 1990, 1993, and 2000 respectively, as well as the M.D. degree from Boston University School of Medicine in 2000. In 2004, he completed his residency in anesthesiology at The Johns Hopkins University in Baltimore, MD, where he also served on faculty in the departments of Anesthesiology & Critical Care Medicine and Biomedical Engineering. His research interests include computational modeling of respiratory mechanics, the design and function of mechanical ventilators and anesthesia machines, patient monitoring, image processing, as well as linear and nonlinear systems analysis.

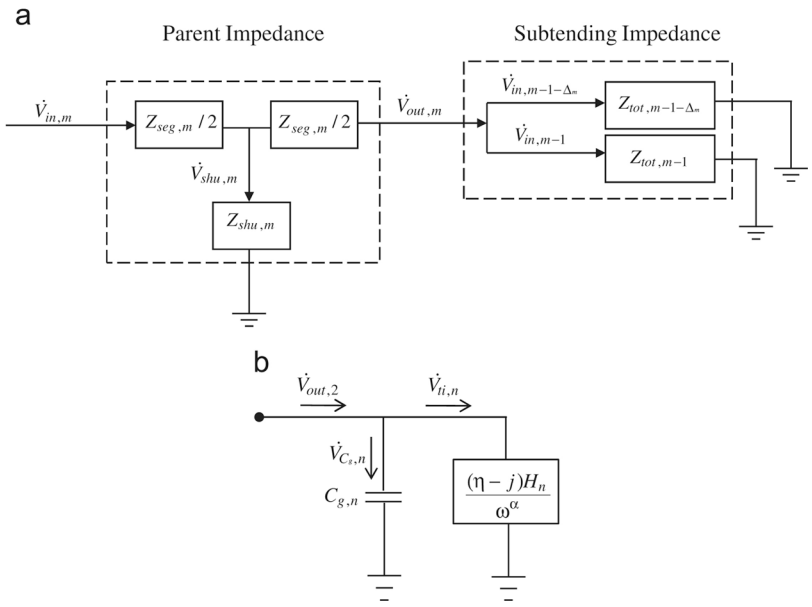

Figure 1.

Computation of flow division at A) representative parent airway segment of order m with daughter segments of orders $m-1$ and $m-1-\Delta_m$; and B) terminal acinar unit n. Flow division at each parent airway segment is dependent upon parallel shunt impedance, $Z_{shu,m}$, as well as the total downstream impedance of each daughter node. Flows are oscillatory, complex quantities with both magnitudes and phases. Pressure distributions are determined from the products of segment impedances and flows. See text for description of variables names.

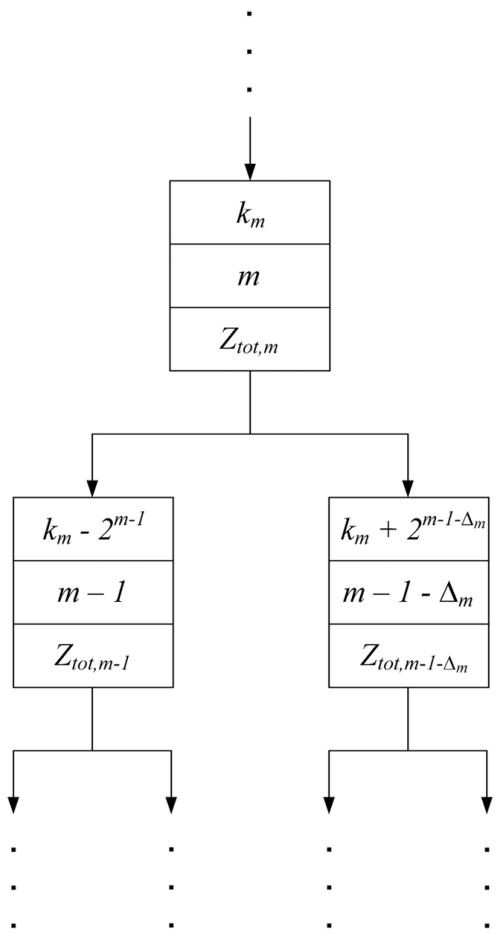

Figure 2.
Example nodes of a parent and two subtending daughter branches from the binary tree data structure. The data record of each node in the tree contains its unique key index k_m, its Horsfield order m [8], and its downstream impedance $Z_{tot,m}$.

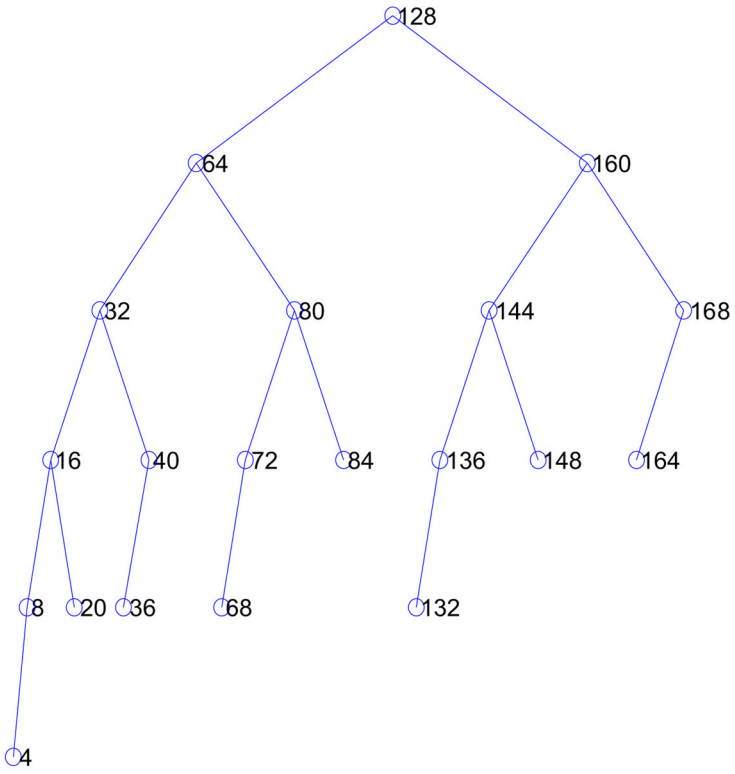

Figure 3.
Example of binary data structure developed using Matlab *Data Structures and Algorithms Toolbox* (available online at http://code.google.com/p/pointer/). The structure utilizes data nodes, pointers, and linked lists arranged to store a binary tree. Each node in the tree is identified by a unique key index, with all variables quantifying airway segment dimensions, downstream impedances, flows, and pressures stored in a data record at each individual node. See text for details.

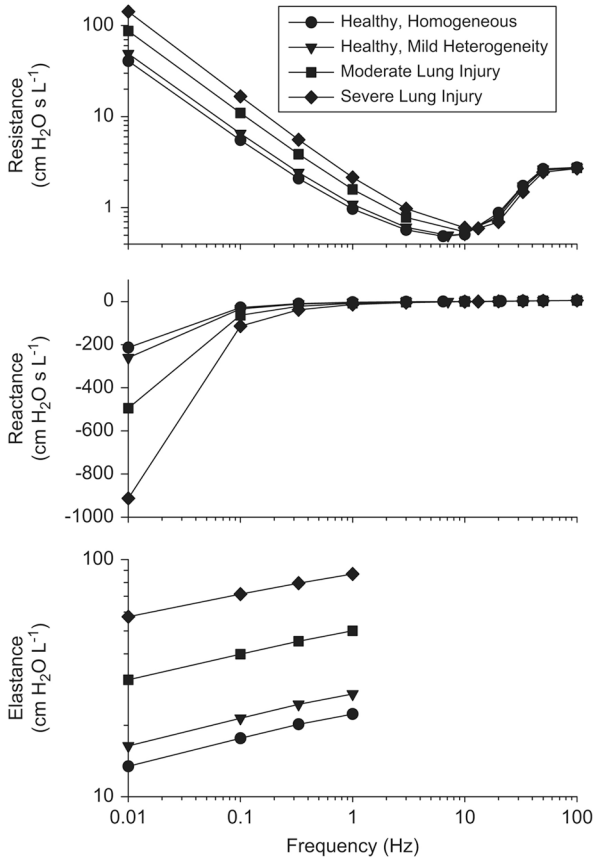

Figure 4.

Total lung input impedance from 0.01 to 100 Hz expressed as resistance, reactance, and elastance for the four different physiologic/pathophysiologic conditions. Elastance is expressed only out to 1 Hz, as above this frequency the effects of gas inertia in the central airways of the model become a more dominant contributor to reactance.

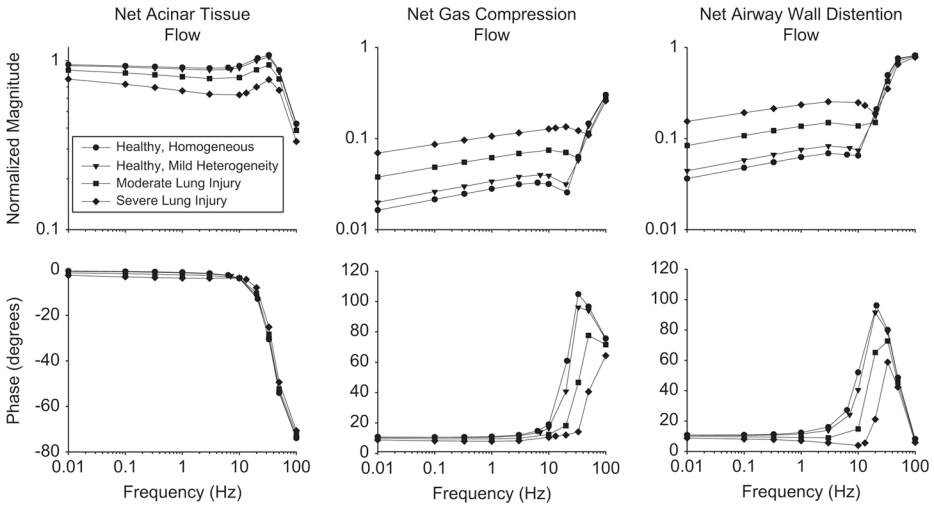

Figure 5.

Summary of partitioning of total tracheal flow into net acinar tissue, gas compression and airway wall shunting components for the four different physiologic/pathophysiologic conditions. Net flows are expressed as magnitudes and phases versus frequency.

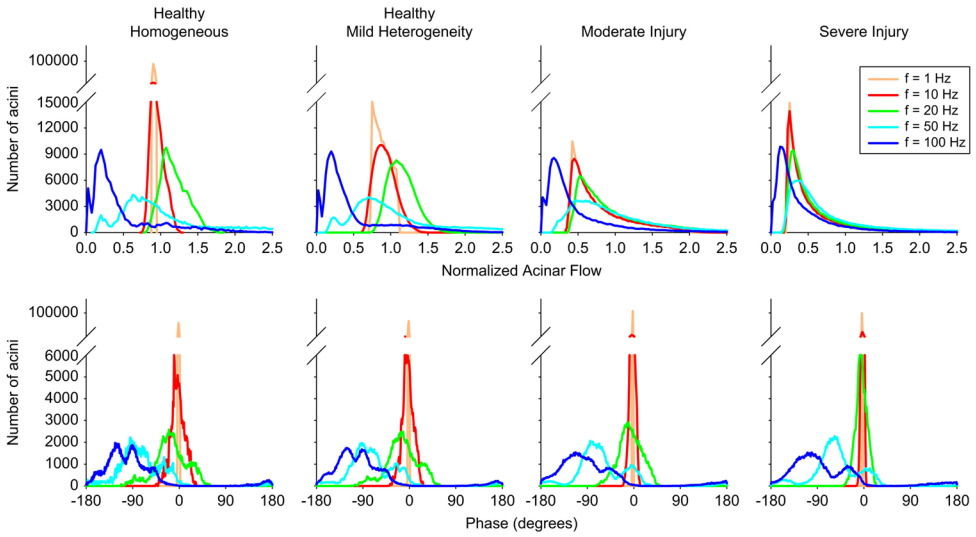

Figure 6.

Histograms of acinar flow distributions for four different physiological conditions and five different frequencies. Magnitudes are normalized relative to what the theoretical flow distribution would be in an entirely homogeneous lung with symmetric branching and rigid airway walls [10]. Phases are expressed relative to tracheal flow.

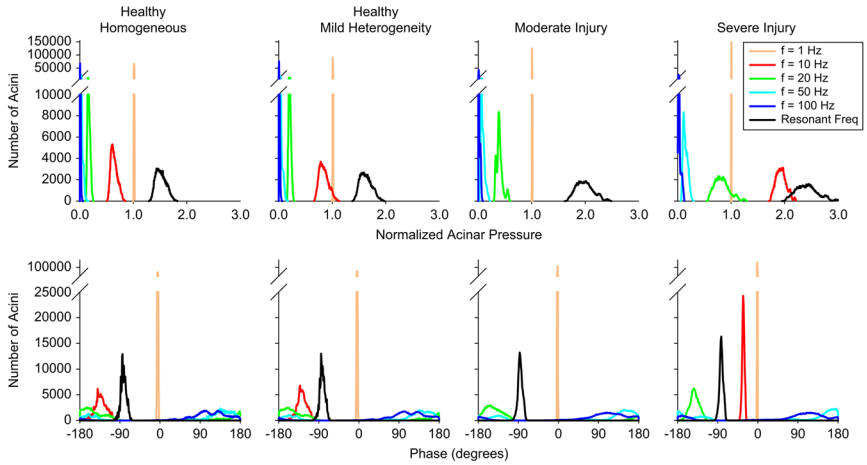

Figure 7.

Histograms of acinar pressure distributions for four different physiological conditions and six different frequencies, including the corresponding resonant frequency. Pressure magnitudes and phases are normalized relative to corresponding tracheal pressure.

Table 1

Maximum elastance (H_{max}) values used for model simulations of four simulated conditions of health and disease. Note that $H_{min} = 20N$ for all simulations. An increase in H_{max} represents an increase in heterogeneity of the parenchymal tissue mechanics.

Condition	$H_{max}N^{-1}$ (cm H_2O L^{-1})
Healthy Homogeneous	20
Healthy, Mild Heterogeneity	30
Moderate Lung Injury	100
Severe Lung Injury	300

Table 2

Resonant frequencies determined from zero-crossings in lung reactance spectra for the four simulated conditions of health and disease.

Condition	Resonant Frequency (Hz)
Healthy Homogeneous	6.4
Healthy, Mild Heterogeneity	7.1
Moderate Lung Injury	10.0
Severe Lung Injury	13.2